Published in final edited form as:
Toxicol Appl Pharmacol. 2008 October 15; 232(2): 190–202. doi:10.1016/j.taap.2008.06.008.

CHARACTERIZATION OF BILIARY CONJUGATES OF 4,4'-METHYLENEDIANILINE IN MALE VERSUS FEMALE RATS

Kan Chen[2], **Richard B. Cole**[2], **Vicente Santa Cruz**[3], **Ernest W. Blakeney**[4], **Mary F. Kanz**[3], and **Tammy R. Dugas, Ph.D.**[1,*]

1*Department of Pharmacology, Toxicology & Neuroscience, Louisiana State University Health Sciences Center – Shreveport, Shreveport, LA*

2*Department of Chemistry, University of New Orleans, New Orleans, LA*

3*Department of Pathology, University of Texas Medical Branch, Galveston, TX*

4*Department of Chemistry, Centenary College, Shreveport, LA.*

Abstract

4,4'-Methylenedianiline (4,4'-diaminodiphenylmethane; DAPM) is an aromatic diamine used in the production of numerous polyurethane foams and epoxy resins. Previous studies in rats revealed that DAPM initially injures biliary epithelial cells of the liver, that the toxicity is greater in female than in male rats, and that the toxic metabolites of DAPM are excreted into bile. Since male and female rats exhibit differences in the expression of both phase I and phase II enzymes, our hypothesis was that female rats either metabolize DAPM to more toxic metabolites or have a decreased capacity to conjugate metabolites to less toxic intermediates. Our objective was thus to isolate, characterize, and quantify DAPM metabolites excreted into bile in both male and female bile duct-cannulated Sprague Dawley rats. The rats were gavaged with [^{14}C]-DAPM, and the collected bile was subjected to reversed-phase HPLC with radioisotope detection. Peaks eluting from HPLC were collected and analyzed using electrospray MS, NMR and FT-IR spectroscopy. HPLC analysis indicated numerous metabolites in both sexes, but male rats excreted greater amounts of glutathione and glucuronide conjugates than females. Electrospray MS and NMR spectra of HPLC fractions revealed that the most prominent metabolite found in bile of both sexes was a glutathione conjugate of an imine metabolite of a 4'-nitroso-DAPM. Seven other metabolites were identified, including acetylated, cysteinyl-glycine, glutamyl-cysteine, glycine, and glucuronide conjugates. While our prior studies demonstrated increased covalent binding of DAPM in the liver and bile of female compared to male rats, in these studies, SDS-PAGE with autoradiography revealed 4–5 radiolabeled protein bands in the bile of rats treated with [^{14}C]-DAPM. In addition, these bands were much more prominent in female than in male rats. These studies thus suggest that a plausible mechanism for the increased sensitivity of female rats to DAPM toxicity may be decreased conjugation of reactive DAPM metabolites, leading to greater levels of protein adduct formation.

*Address correspondence to Tammy Dugas, Department of Pharmacology, Toxicology & Neuroscience, LSU Health Sciences Center-Shreveport, 1501 Kings Highway, Shreveport, LA 71130. email: tdugas@lsuhsc.edu.

Keywords

Methylene dianiline; bile duct cells; xenobiotic metabolism; sex differences; conjugation; glutathione; biliary excretion

INTRODUCTION

4,4'-Diaminodiphenylmethane (DAPM, 4,4'-methylenedianiline) is an aromatic diamine used as a precursor to 4,4'-methylenediphenyldiisocyanate (MDI) in the production of a number of polyurethane products. The toxicity of DAPM was first documented following the Epping jaundice incident of 1964, in which 84 people accidentally consumed DAPM and subsequently suffered symptoms of toxic hepatitis (Kopelman et al., 1966). This and other accidental and occupational exposures to DAPM have resulted in fever, jaundice, toxic hepatitis, cholangitis with cholestasis, skin rash, and in two acute cases, cardiomyopathy and retinopathy (Brooks et al., 1979; McGill et al.; 1974; Bastian, 1984). In rats, chronic treatment with DAPM increased the incidence of thyroid and hepatic carcinomas (Weisburger et al., 1984; Lamb et al., 1986). Although studies of acute DAPM exposure indicated that biliary epithelial cells of the liver and common bile duct are the early site of injury (Kanz et al., 1992, 1995) little is known about its mechanism of toxicity. One prerequisite for elucidating the mechanism of DAPM toxicity is an understanding of its metabolism.

Current knowledge about DAPM metabolism has been ascertained from the characterization of metabolites isolated from rabbit, rat or human urine following DAPM exposure (Cocker et al., 1986, 1988a; Morgott, 1984). The major urinary metabolite found in humans and in rabbits exposed to DAPM is *N*-acetylated DAPM (Cocker et al., 1986, 1988a) This metabolite was also found to be the major metabolite conjugated to hemoglobin in humans (Bailey et al., 1990). *N*-acetylation has therefore been proposed as one major pathway in the metabolism of DAPM in humans. In addition to the acetylated metabolites, Kautiainen et al. (1998), demonstrated a hemoglobin adduct to a DAPM imine, formed following treatment of rats with DAPM. Because they were able to generate a similar product by incubating DAPM with peroxidase enzymes, they hypothesized that the imine was formed by extrahepatic peroxidases.

While these studies identified metabolites in urine and blood, the possibility exists that different, perhaps more reactive, metabolites of DAPM are excreted into bile, the proposed route of bile duct epithelial cell exposure to the proximate toxicant of DAPM (Kanz et al., 1995). Biliary excretion is an important mechanism for the elimination of xenobiotics. Conjugates formed following phase II reactions are the most common types of metabolites excreted in bile (Klaassen et al., 1984). Thus, it is highly likely that reactive metabolites of DAPM formed following phase I oxidation reactions would be excreted into bile once they become conjugated, e.g., to glutathione, glucuronic acid, or even protein (Hobara et al., 1988).

Recent studies conducted in our laboratory demonstrated an increased sensitivity of female compared to male rats to DAPM-induced hepatobiliary injury (Dugas et al., 2001). Sex differences have been documented in metabolism involving isoforms of cytochrome P450 (Mugford et al., 1998; Sundseth *et al*., 1992; Skett, 1988) sulfotransferases (Mugford et al., 1998), esterases (Los *et al*., 1996), as well as glucuronyl and glutathione-*S*-transferases (Zhu et al., 1996; Rao et al., 1977) and glutathione (Srivastava, 1993). Thus, we hypothesize that the greater susceptibility to injury observed in female rats is due to differences in DAPM metabolism between the sexes. The aim of this study is to isolate, identify, and compare metabolites of DAPM excreted into the bile of male and female rats.

EXPERIMENTAL PROCEDURES

Materials

DAPM (4,4'-diaminodiphenylmethane) was purchased from Aldrich (Milwaukee, WI), and aromatic ring-labeled [^{14}C]-DAPM (specific activity 6.8 mCi/mmol) was synthesized by American Radiolabeled Chemicals (St. Louis, MO). Unless otherwise noted, all other chemicals and reagents were obtained from Sigma Chemical Co. (St. Louis, MO) and were of analytical grade or higher. Stock solutions of DAPM containing 2–4% [^{14}C]-DAPM were dissolved with gentle warming in absolute ethanol and then diluted with deionized water to achieve a final concentration of 12.5 or 25 mg/mL DAPM in 35% ethanol. All doses of DAPM were administered at 2 mL/kg volumes.

Methods

Animals—Male and female Sprague Dawley (Harlan, Indianapolis, IN) rats of similar ages (12–15 weeks) were housed under controlled temperature and humidity (18–21°C, and 55 ± 5%, respectively). All animals were maintained in wire-bottomed cages over absorbent paper in 12 hour light/dark cycles and were acclimated to the animal room for at least one week prior to DAPM treatment. [^{14}C]-DAPM or vehicle was administered to a total of 16 male (330–380 g) and 18 female (290–310 g) rats for the assessment of biliary metabolite excretion.

Animal surgery and bile collection procedure—Rats were anesthetized with pentobarbital (50 mg/kg, i.p.) and biliary, duodenal, and peritoneal cannulas were implanted by standard procedures (Dugas et al., 2001; Kanz et al., 1995). Following surgery, taurocholate was infused into the duodenum to maintain continuous bile flow for 6–8 h, and when needed, pentobarbital diluted with saline was infused slowly into the peritoneum. Animals were equilibrated to stabilize physiological parameters such as respiration and body temperature, and basal bile was collected for 1 hour at 15 min intervals. Rats were next gavaged with either 25 or 50 mg/kg [^{14}C]-DAPM, or vehicle (35% ethanol), and bile was collected for an additional 6 hours in tared tubes stored on dry ice (Dugas et al., 2001). Bile samples thus collected were stored at −80°C until analysis.

Metabolite profiling in rat bile was conducted either by fractionation after HPLC separation, followed by MS^n analysis, or by employing LC/ESI-MS^n. Separation and detection of the radioactive metabolites were performed by HPLC coupled to both UV and radioisotope detection. Once the retention time of each [^{14}C]-DAPM metabolite was identified, non-radiolabeled metabolites were collected, and these fractions were characterized by mass spectrometry.

HPLC fractionation of [^{14}C]-DAPM metabolites—Bile samples collected from the first 15 min of each half hour after DAPM treatment were evaluated for the presence of radiolabel using liquid scintillation counting. Bile samples collected from alternate 15 min intervals and determined to contain radiolabeled DAPM were thawed, deproteinized using Microcon 10,000 MW centrifugal filters (Fisher Scientific, Houston, TX), and then 20–50 μL samples were immediately injected onto HPLC. Alternatively, for some samples, 20 μL was injected and was directly analyzed using LC/ESI-MS^n. The collected fractions were concentrated by freeze-drying and reconstituted in a small volume of acetonitrile: water (50:50) for MS^n analysis. During the course of these studies, we noted that any additional incubation even at 4°C resulted in increased numbers of peaks on HPLC, suggesting rapid decomposition of metabolites. The chromatography was accomplished using a Waters (Milford, MA) 626 pump and a 2487 dual-wavelength UV detector interfaced to an INUS Systems (Tampa, FL) β-RAM radioisotope detector. The separation was achieved using a 250 × 4.6 mm Ultrasphere (Beckman-Coulter, Fullerton, CA) reversed phase C18 column, a flow rate of 0.5 mL/min, and the following elution

program: 1) gradient elution from 80% A (50 mM ammonium acetate, pH 3.5)/ 20% B (100% methanol) to 70% A/ 30% B over 10 min, then to 57% A/ 43% B over 35 min, and lastly to 50% A/ 50% B over 15 min; 2) isocratic elution at 50% A/ 50% B for 5 min; 3) gradient elution to 100% B over 35 min; and 4) isocratic elution at 100% B for 5 min. Sample elution was monitored using Millenium 32 software (Waters), with UV detection at 254 nm and radioisotope detection run on separate channels. After all peaks had eluted, the column was washed with methanol and was re-equilibrated with 80% A/ 20% B before injecting the next sample. In some experiments, peaks eluting from the HPLC were collected on dry ice and were stored at −80°C until analysis by electrospray MS or NMR.

Quantitation of individual metabolites was determined for each rat over the period of bile collection. First, the levels of metabolite (nmol) detected over a given 15 min interval were plotted versus minutes after DAPM treatment, and then the areas under the curves (AUC) were calculated using GraphPad Prism software. Finally, the AUC for each metabolite were averaged over the treatment group.

Mass spectral characterization of biliary metabolites—After HPLC fractionation, MS analysis was performed by infusion injection at a flow rate of 1μL/min on a Thermo Finnigan LCQ Deca XP MAX ion trap mass spectrometer equipped with a nanospray ion source from New Objective (Woburn, MA) and an uncoated nanospray TaperTipTM (Tip ID 75μm, New Objective). For continuous infusion, 2.8kV was applied on the nanospray needle and the temperature of the heated transfer capillary was 200°C. Structural analysis of the selected ions was performed by MS^n with relative collision energy between 30 – 45 % and with an activation time of 5 – 30 msec.

Alternatively, after protein removal, metabolite characterization was conducted using LC/ESI-MS^n with 20 μL sample loading. The column used for the separation was an XTerra-MS C18 reversed phase column (1.0 × 150 mm, 3μm, Waters). The mobile phase consisted of 10 mM ammonium acetate buffer, pH 3.5 (mobile phase A) and acetonitrile (mobile phase B). A gradient program, run at a flow rate of 50 μL/min, began with 15% B for the first 2 min, which was increased to 30% at 35 min, and then to 90% at 40 min using a linear gradient, with a hold from 40 to 45 min.

For LC/ESI-MS^n data acquisition, the LCQ was operated in data dependent mode with dynamic exclusion enabled where the highest peak in every MS scan (mass range: m/z 100 – 700 Da) was subjected to MS/MS analysis. The six largest peaks in the MS^2 spectrum were selected for the MS^3 experiment. Dynamic exclusion was set to repeat count = 2, repeat duration = 0.3 min, exclusion duration = 0.4 min, and exclusion mass width = 3 m/z. The temperature of the heated capillary and the spray voltage were 275°C and 3.2 kV, respectively, the sheath gas flow rate was 35 units, and the capillary voltage was set at 27 V.

NMR characterization of [^{14}C]-DAPM metabolites—Metabolites in samples used for NMR analyses were first separated by the HPLC procedure described above, except that running buffer A consisted of 80 mM phosphate buffer, pH 3.5. This change in running buffer produced little variation in peak retention time, but did allow for the NMR characterization of metabolites without interference from organic salts. The peak eluting at 43.7 min was collected from 4 samples, was pooled and was stored on dry ice. The aqueous sample was freeze-dried in a Virtis Genesis 12SL lyophilizer using condenser and shelf temperatures of −45°C and −20°C, respectively. For 1-D ^{1}H NMR experiments, samples thus dried were dissolved in d_6-dimethylsulfoxide (Cambridge Isotope Laboratories) and were run nonspin at 25°C on a Varian Unity *plus* 750 MHz NMR spectrometer. For comparison, ^{1}H NMR spectra were also acquired for three reference samples – nitrosobenzene, 4,4'-methylenedianiline, and 4,4'-diaminobenzophenone – dissolved in d_6-DMSO. Two dimensional TOCSY (Total Correlation

Spectroscopy) spectra were acquired using a Varian Unity+ 400 MHz NMR as a phase sensitive data set of 256 increments of 128 scans and 2048 data points each. A pulsed spin-lock field of 6.9 KHz was applied for a mix period of 80 msec, with a relaxation delay of 2.3 sec and sweep width of 4.8 KHz in both dimensions. Shifted sine-bell apodization was used in both dimensions and zero filling to a 4K by 4K matrix was performed prior to 2D Fourier transformation.

SDS polyacrylamide gel electrophoresis of radiolabeled biliary protein—A 10% polyacrylamide gel was prepared. Samples of bile were diluted 1:1 with blue solution containing 50% glycerol, 2% sodium dodecyl sulfate, and 0.05% bromphenyl blue. Gels were then loaded with 30 μL bile/well and were electrophoresed at 40 A for ~1.5 h. Gels were fixed with 20% methanol/ 10% acetic acid for 30 min and were washed for 30 min in 20% methanol. To enhance the radioactive fluor, the gel was then treated with 0.5 M sodium salicylate in 20% methanol (containing 2% glycerol) for 30 min. Additional glycerol (final concentration = 10%) was added 3 min before the end of the treatment period. The gel was then dried, placed on X-ray film, and stored at −80°C for 2–3 weeks before film processing.

Statistics—Values given in Table 2 represent means ± SEM. Statistical analyses of these data were performed using SPSS for Windows (San Diego, CA). Significant effects of dose and sex were assessed using two-way ANOVA. Significance between individual data points was determined post-hoc using Bonferonni, Tukey's, and LSD t-tests. In all cases, $p < 0.05$ was accepted as statistical significance.

RESULTS

The number of metabolites apparent by HPLC (Figure 1) varied dramatically between rats; however, overall the number of metabolites did not vary between sexes. The metabolites displayed a range of polarities, from relatively polar (eluting at 21.6 min) to nonpolar (eluting at 89 min). The most prominent metabolite by far in both male and female rats eluted at 43.7 min. Other prominent metabolites found in both sexes eluted at 40.5, 42.1, 48, 55, 67, 85, and 89 min.

The remarkable reactivity of the metabolites should be noted. Careful attention to maintaining the samples at a significantly reduced temperature during preparation was required. Any additional incubation of the sample beyond that described in Materials and Methods, even at 4°C, resulted in approximately twice the numbers of peaks by HPLC. This observation may be due to the reaction of DAPM metabolites with other biological molecules (e.g., peptides) not eliminated by the protein filtration procedure.

Characterization of metabolites by MS

The HPLC-radioisotope chromatogram (RIC) revealed several metabolites. Those that were adequately characterized are labeled as metabolites M1–M9 in Scheme 1. Structural assignments of the metabolites were made using mass spectral and NMR data, as well as LC/MS^n data acquired for the same metabolites derived from non-radiolabeled DAPM. Several additional metabolites are shown in the HPLC-RIC (Figure 1). However, for these, tandem spectral data did not afford a clear structural assignment. Therefore, these data are not presented. The LC/MS analysis had an advantage over HPLC-RIC fractionation in that metabolites could be separated by both their hydrophobicity, using a reversed phase column, and by their differing m/z values. For example, although M1–M3 and M8–M9 could not be separated using HPLC-RIC (Figure 1), the metabolites could be adequately separated and characterized by LC/MS^n. The totality of the MS and NMR data collected indicate that DAPM is biotransformed *via* phase I and II metabolism (Scheme 1), including hydroxylation,

oxidation, acetylation, glucuronidation, glycine, and glutathione conjugation. The individual spectra used to characterize metabolites M1–M9 are described below.

Metabolite 1—The mass spectrum showed an MH^+ at m/z 375, with fragment ions at m/z 357 (-H_2O), 339 (-2 H_2O), 321 (-3 H_2O) and 199 (-176 amu) (Figure 2). Note that a loss of 176 m/z is typical of a glucuronide conjugate (Clarke et al., 2001). The presence of this characteristic loss was also used in the identification of M6 and M7. Further MS/MS fragmentation (MS^3) of m/z 199 showed an identical tandem mass spectrum as DAPM, producing two major fragment ions at m/z 106 and 182 (Figure 2).

Metabolite 2—The mass spectrum of this apparent glutathione conjugate showed a protonated molecule at m/z 532 (Figure 3A). The tandem mass spectrum of this precursor elicited fragment ions at m/z 457 (-glycine), 439 (-glycine -H_2O), 403 (-pyroglutamate), 385 (- pyroglutamate -H_2O), 300, 308, 283, 257, 225 and 199, 179 (protonated cysteinylglycine). Since the fragment ion at m/z 300 was postulated to contain xenobiotic structural information, an MS^3 spectrum was acquired. M/z 300 was produced by the loss of both glycine and glutamate residues from the precursor m/z 532. Further fragmentation of m/z 300 gave product ions at m/z 106, 199, 225, 257 and 283 (Figure 3B). This latter figure and the proposed fragmentation pathways depicted in Scheme 2 show that many informative fragments containing the xenobiotic moiety can be produced from consecutive decompositions of m/z 300.

Metabolite 3—An apparent cysteinyl-glycine conjugate derived from metabolite 5 produced MH^+ at m/z 403 (Figure 3C). MS/MS of the parent ion at m/z 403 gave fragment ions at m/z 179 (protonated cysteinyl-glycine), 199, 225, 300, 310 and 385 (-H_2O).

Metabolite 4—A putative glutamyl-cysteine conjugate similar to metabolites 2 and 3 produced an MH^+ ion at m/z 475 (Figure 3D). The MS/MS spectrum of the precursor ion at m/z 475 showed fragment ions at m/z 199, 225, 283, 300, 346 (-pyroglutamate) and 457 (-H_2O). The likely mechanisms for fragmentation of molecular ions for metabolites 3 and 4 are shown in Scheme 2.

Metabolite 5—N-acetyl-DAPM, previously characterized in urine and in DAPM-treated vascular cells (Chen *et al*., 2006; Cocker et al., 1988b) was also found in the excreted bile. MS/MS analysis of MH^+ at m/z 241 produced fragment ions at m/z 106 and 148 (data not shown). Additionally, an ammonium adduct and a protonated N-acetyl-DAPM dimer ion were also observed at m/z 258 and 481, respectively. A tandem mass spectrum of precursor m/z 481 showed a fragment ion at m/z 241. Further MS^3 analysis produced fragment ions at m/z 106 and 148. Fragmentation of the parent ion at m/z 258 resulted in an ion at m/z 241, which when subjected to MS^3 analysis, produced fragment ions at m/z 106 and 148 (data not shown).

Metabolite 6—The mass spectrum of metabolite 6 showed an MH^+ at m/z 417, representing a glucuronide conjugate of N-acetyl-DAPM (Figure 4). MS/MS of the parent ion at m/z 417 elicited fragment ions at m/z 399 (-H_2O), 381 (-2 H_2O), 363 (-3 H_2O) and 241 (-176 amu). The major fragment ion at m/z 241 was formed by the characteristic loss of the glucuronic acid moiety from the parent ion. MS^3 fragmentation of the ion at m/z 241 produced two major product ions at m/z 106 and 148, a pattern that was identical to the tandem mass spectrum of N-acetyl-DAPM (M5).

Metabolite 7—A major metabolite was found at m/z 478, with a characteristic neutral loss of 176 amu and a subsequent water loss from the parent ion in the MS/MS experiment, indicating a glucuronide conjugate had formed (Figure 5A). MS/MS of the protonated

glucuronide conjugate (m/z 478) gave fragment ions at m/z 460 (-H_2O), 442 (-2 H_2O), 302 (-176, loss of glucuronic acid moiety) and 285 (-176 -NH_3). Further MS/MS of the fragment ion at m/z 285 produced daughter ions at m/z 106, 148, 150, 241 and 267. A mechanism for fragmentation m/z = 478 is proposed in Figure 5B.

Metabolite 8—A second glutathione conjugate found in rat bile produced a protonated molecule ion at m/z 574 (Figure 6). The MS/MS spectrum of the parent ion at m/z 574 showed fragment ions at m/z 445 (-pyroglutamate), 499 (-glycine), 342, 325, 283, 267 and 241. Proposed pathways for decompositions of M8 are shown in Scheme 3.

Metabolite 9—Metabolite 9, identified as a cysteinyl-glutamate conjugate derived from metabolite 8, gave MH^+ at m/z 517 (data not shown). The MS/MS spectrum of the parent ion at m/z 517 demonstrated fragment ions at m/z 241, 267, 283, 325, 342, 388 (-pyroglutamate), and 499 (-H_2O).

Characterization of metabolites by NMR

Relatively pure quantities of metabolite 2 obtained by HPLC fractionation were analyzed by ^{1}H-NMR spectroscopy (Figure 7A). Note that only metabolite 2 was sufficiently abundant for its adequate characterization by NMR. Chemical shifts and splitting in the aliphatic region of the ^{1}H NMR spectrum for metabolite 2 were in agreement with those observed for glutathione (Figure 3A), both in our laboratory and in prior reports (Ellis *et al*., 1992; Mutlib *et al*., 1999). Chemical shifts for protons were assigned and their respective multiplicities were denoted as follows: s = singlet; d = doublet; t = triplet; m = multiplet; dd = doublet of doublet. Using these assignments, the chemical shifts and multiplicities for metabolite 2 were 1.91 ppm, m; 1.92, m; 2.28, m; 2.49, s; 2.39, dd; 2.58, dd; 3.69, m; 4.42, d; 6.46, d; 6.82, d; 7.36, d; 7.08, d; 8.37, d; 8.63, m; 10.25, s. By comparison, the chemical shifts and multiplicities for glutathione used as a standard were 1.90 ppm, m (Glu β); 2.35, m (Gluγ); 2.48, s (DMSO); 2.68, dd (Cys β); 2.81, dd (Cys β); 3.39, m (Glu α); 3.7, m (Gly α); 4.38, m (Cys α).

In addition, four sets of doublets were observed in the aromatic region of the ^{1}H spectrum (6.46–7.08 ppm) for metabolite 2. The protons on both phenyl rings appear unaffected by metabolism, but they do show differing chemical shifts resulting from the loss of symmetry in comparison with the structure of DAPM. Thus, oxidation of at least one of the amino groups likely occurred, with the resulting nitroso group withdrawing electron density on one phenyl ring and shifting its protons (a and b) down-field (see NMR spectrum; Figure 7A). The appearance of an MS^3 fragment ion at m/z 106 Da (Figure 3B), representing the 4-nitroso-phenyl moiety, further corroborates our assignment of oxidation on one amino group in the DAPM structure.

To rationalize the observation of other proton chemical shifts (c and d) below 7 ppm and to explain the mass difference between the DAPM parent compound and the metabolite observed in the mass spectrum for metabolite 2, the formation of an imine on the other aniline moiety of DAPM and hydroxylation of the methylene linkage carbon seems to be the most plausible. The chemical shift of proton e (δ = 10.2) from the methylene bridge hydroxyl group supports this assignment, since the neighboring functionalities should force the proton down-field (predicted using Chemical Office Ultra 2004 software, Cambridgesoft Corporation). Additionally, long distnce coupling between proton e (δ = 10.2) and proton b (δ = 7.0) is observed in the 2D TOCSY NMR experiment (Figure 7B). While presumably both the keto-amine and the enol-imine structures exist in the sample as keto-enol tautomers (see Scheme 1), the enol form is more obvious from both the mass spectral and NMR data.

Lastly, in considering the site of attachment of glutathione, conjugation could occur through formation of an S-C bond on the ring carbon adjacent to the imine nitrogen atom, or through

formation of an S-N bond directly on this same nitrogen. However, the former is in irresolvable conflict with the total nominal mass of the protonated glutathione adduct (m/z 532) measured by mass spectrometry. Thus, we can definitively assign the glutathione linkage as an S-N bond with the imine (Figure 3A, Figure 7A).

Quantitation of DAPM metabolites

Area under the curve (AUC) analysis revealed that for metabolites M3/M4, M2, M5, M6, and M7, representing acetylated, glucuronide and glutathione (as well as CysGly and GluCys) conjugates, biliary excretion was greater in male compared to female rats (Table 1). This trend was consistent for both the 25 and the 50 mg/kg doses, but the effect was statistically significant for all of the metabolites except M2 at the 25 mg/kg dose (Table 1). The identities of all nine metabolites appearing in Figure 1 and Table 2 (M1–M9) were verified by tandem mass spectral analysis of collected HPLC fractions. The peak eluting at 21.6 min matched the retention time for our DAPM standard, thus, it was tentatively assigned as unmodified DAPM, even though mass spectral characterization of this compound was not possible due to poor signal strength. Nevertheless, for this latter compound, biliary excretion in males was likewise greater than that in female rats (Table 1).

Amounts of radiolabeled protein excreted into bile

Gels were loaded with equivalent amounts of bile from rats treated with 50 mg/kg [^{14}C]-DAPM. Previous studies (Kanz et al., 1998) had shown that biliary protein excretion increased with time following DAPM treatment. Thus, for each gel, male and female rats were chosen such that the biliary protein was not different between the two rats compared; i.e., biliary protein concentration at 2h in the female rat was equivalent to biliary protein concentration at 2h in the male rat. A representative gel from such a comparison is presented in Figure 8. Autoradiography of the gels showed 5–6 bands in both sexes, with much more radiolabel bound to protein in the female rats as compared to male rats. This increased level of protein binding of radiolabeled DAPM in female rats was reproducible in each set of rats tested. Importantly, if samples for loading were prepared using dithiothreitol (DTT), all radioactivity was concentrated along the dye front, with no radiolabeled bands apparent elsewhere on the gel.

DISCUSSION

For both sexes, the majority of DAPM/DAPM metabolite was excreted in bile within the first 2 – 2 ½ hours (Dugas et al., 2001). Our prior experiments demonstrated that at the 25 mg/kg DAPM dose, biliary excretion of metabolite was greater in male rats than in females, reaching a maximum rate of ~18 μg/min*kg in males and ~9 μg/min*kg in females at 15 and 45 min, respectively (Dugas et al., 2001). However, these marked differences in biliary excretion of metabolites observed between the sexes were not due to significant differences in bile flow. In contrast, at the 50 mg/kg DAPM dose, biliary excretion of metabolite was comparable between males and females, and reached a maximum rate of ~9 μg/min*kg at 45 min (Dugas et al., 2001). In these prior studies, we determined that the threshold dose for observing injury was 25 mg/kg for female rats, and 50 mg/kg in males. We rationalized that at the 25 mg/kg dose, males were capable of efficiently metabolizing and excreting DAPM, but at the higher dose, metabolism was compromised. On the other hand, in females, efficient metabolism and excretion of DAPM was compromised at either dose. Thus, we hypothesized that in female rats, even though less metabolism of DAPM occurred, DAPM was either metabolized to more toxic intermediates or detoxication pathways were compromised. To test this hypothesis, we characterized and quantitated 9 DAPM metabolites excreted into bile in female versus male rats at both doses.

Structural characterization of DAPM metabolites

The most prominent metabolite excreted in the bile of rats treated with DAPM was metabolite 2 eluting at 43.7 minutes, which we have characterized as a glutathione conjugate. Data supporting this conclusion include the appearance of a $[CysGly + 2H]^+$ fragment and losses of $[Glu]^+$ and $[Cys]^+$ in the LC/MS, and chemical shifts and splitting in the aliphatic region (1–5 ppm) similar to those reported for glutathione (Ellis et al., 1992) on ^1H NMR. The molecular ion provided by mass spectrometry ($[M + H]^+ = 532$ amu) suggested that in addition to glutathione conjugation, the metabolic pathway in the formation of M2 from DAPM involved a loss of five protons and a gain of two oxygen atoms.

Still uncertain, however, was the identity of the downstream 10.25 ppm chemical shift observed in the ^1H NMR. This shift could be designated as a free carboxylic acid proton on the glutathione moiety, but prior reports for the NMR analysis of glutathione metabolites did not indicate this particular shift (Ellis et al., 1992; Mutlib et al., 1999), presumably due to exchange with deuterated solvent. In our case, while it was apparent from the symmetry of the observed chemical shifts and splitting in the aromatic region of the spectrum that the GSH molecule must be linked to the metabolite through one of the aromatic amine functional groups, our original hypothesis was that this unusual downstream shift (10.25 ppm) was derived from a lone proton on the aromatic amine (aromatic-NH-S- of the keto-amine). Although the possibility of a proton on an aromatic amine nitrogen seemed possible from the NMR spectrum, the observed fragmentation pattern observed in the mass spectral experiment (Scheme 3) made the enol-imine structure seem more plausible. Use of Chemical Office Ultra 2004 software (Cambridgesoft Corporation) to predict the chemical shift of the type of hydroxyl proton that would exist in the enol-imine structure would indeed exhibit a down-field shift.

To confirm our hypothesis for the structure of M2, we performed TOCSY two-dimensional NMR to ascertain whether there was coupling between the proton of interest (10.25 ppm) and protons on the aromatic ring that were *ortho* to the methylene bridge. TOCSY did in fact indicate some weak coupling between shifts at 10.2 and 7.1 ppm, thus confirming this proton was situated adjacent to the ring. We therefore assign the structure of M2 as the nitroso-glutathione metabolite indicated in Scheme 1. However, though the compilation of mass spectral and NMR data more strongly suggest an enol-imine, this structure undoubtedly exists as a tautomer of a keto-amine.

We can make a few reasonable assumptions about the mechanism for formation of this DAPM conjugate. First, the amine functionality is not terribly electrophilic, so glutathione conjugation likely involves at least one intermediate step. Cases of other similar metabolic pathways have been described in which the amine is first metabolized to a nitroso intermediate that then undergoes nucleophilic addition of glutathione to a glutathione-conjugated *N*-hydroxylamine (Mulder et al., 1982). The hydroxylamine, however, is unstable in aqueous solutions containing glutathione, and thus, the *N*-hydroxylamine is quickly reduced to a glutathione-conjugated imine (Mulder et al., 1982). It is possible that M2 might also have been derived from glutathione conjugation to first an *N*-hydroxylamine, that in turn is reduced to generate the end metabolite identified here as M2.

Among the many metabolites identified in these studies were cysteinyl conjugates. Because biliary epithelial cells lining the bile duct express the enzyme γ-glutamyltransferase (γ-GGT) (Manson, 1983), glutathione conjugates excreted into bile may be expected to undergo cleavage of its terminal glutamate residue to yield CysGly conjugates. Also observed, however, were two GluCys conjugates (metabolites 4 and 9, Scheme 1). These GluCys conjugates are likely not the product of enzymatic cleavage in the bile duct epithelium, but rather, may result from non-enzymatic addition of a γ-GluCys thiol to an electrophilic amine. γ-GluCys is a building

block in the synthesis of glutathione (Wu *et al*., 2004). Thus, appreciable cellular levels of γ-GluCys are likely present.

It should be pointed out that full confirmation of M8 was not possible by mass spectrometry alone. Another plausible structure that could satisfy the mass spectral data and the observed molecular ion would be the addition of glutathione to the ring instead of on the imine nitrogen. Unfortunately, high-magnetic field (i.e., 750 or 800 MHz) NMR was not sufficient for the characterization of the very small amount of metabolite present in even pooled samples, and long acquisition times were complicated by sample degradation. However, circumstantial evidence logically suggests that the M8 structure shown in Scheme 1 has undergone a stepwise combination of biotransformations that are observed in certain of the other metabolites. The most plausible pathway seems to be a P450-mediated oxidation of acetylated DAPM (M5) to generate an intermediate imine (Scheme 1, right column, middle structure) that could undergo nucleophilic attack by the glutathione thiol to generate the proposed structure for M8. This type of intermediate imine formation is a common motif among metabolites M2–4. Two other conjugation pathways were suggested in this work – glucuronidation and acetylation – and these might also be important detoxication pathways for DAPM. Acetylation was previously reported to be a prominent pathway for DAPM metabolism in humans, with acetylated DAPM representing the vast majority of metabolite excreted in the urine of individuals after occupational exposure (Cocker et al., 1994). Glucuronidation was also predictable, as it has been reported as an important conjugation route for benzidine (Lynn et al., 1983), a structurally similar amine.

Also of interest was the characterized glycine conjugate of DAPM (M7). Similar types of amino acid conjugation with either serine or proline have been shown to occur for *N*-hydroxylamines, with the reaction catalyzed by the respective seryl and prolyl t-RNA synthetase enzymes (Kato et al., 1994). However, to our knowledge, the participation of a glycyl t-RNA synthetase in the glycine conjugation of an *N*-hydroxylamine has not been reported. Since glycyl, seryl and prolyl t-RNA synthetase are all members of the class II t-RNA synthetases, they share common catalytic folding patterns, sequence motifs, and mechanistic features (Eriani et al., 1990). Hence, the enzymes may also share a common non-cognate activity. An understanding of non-cognate functions for these enzymes is just now beginning to surface, but a recent report suggests that one function of seryl-tRNA synthetase in *Streptomyces viridifaciens* is in the synthesis of the antibiotic valinimycin (Garg et al., 2006). The mechanism for its synthesis apparently involves the seryl-t-RNA synthetase-mediated conjugation of serine to isobutyl-*N*-hydroxylamine, formed as a metabolite of valine. Thus, amino acid conjugation of an *N*-hydroxylamine may be a non-cognate function of the class II enzymes. It is furthermore possible that the glycine conjugate M7 may represent a bioactivation pathway for DAPM metabolism, since seryl or prolyl conjugates of other *N*-hydroxylamines have been shown to induce DNA adduct formation (Hashimoto et al., 1981). In these earlier studies, amino acid conjugation of *N*-hydroxylamines was shown to promote mutagenesis and DNA adduct formation, likely due to electrophilic nitrenium ion formation following degradation of the *N*-ester of the conjugate (Hashimoto et al., 1981).

Sex differences in the biliary excretion of DAPM metabolites

Our hypothesis for the observed sex differences in DAPM toxicity was that either DAPM was metabolized to more toxic metabolites in female as compared to male rats, or that detoxication, perhaps through conjugation, was compromised in the female rats. HPLC analysis of biliary metabolites excreted in male versus female rats revealed that overall, females excrete significantly less of the conjugated metabolites than males (Table 1). Although there was a trend toward an increased level of conjugates 3/4, 6 and 7, at the low compared to the high

dose in male rats, these differences did not achieve statistical significance. Thus, the dominant effect detected was that of sex and not dose.

The observation that the most prominent biliary metabolite by far was a glutathione conjugate suggests that glutathione conjugation is an important pathway in DAPM metabolism in the liver. This argument is strengthened by our findings on SDS PAGE. Since DTT was able to completely strip our radiolabel from the observed bands (Figure 8), it is reasonable to assume that proteins identified on the gel are bound through thiol residues. Taken together with the preponderance of conjugates derived from glutathione or related pathways, our prior studies suggesting the importance of glutathione levels in protecting against DAPM-induced hepatobiliary toxicity (Kanz et al., 2003), as well as the fact that the expression levels of many isoforms of glutathione-*S*-transferases are 2–3-fold higher in males than in females (Srivastava, 1993), it is reasonable to assume that the sex-dependent differences in sensitivity to DAPM toxicity may be due to a diminished capacity to form glutathione and other conjugates. Both acetylated (M5) and glucuronyl metabolites (M6 and M7) were shown to be present in larger concentrations in the bile of males as compared to females, suggesting that deficiencies in these conjugation pathways might also be critical for the increased sensitivity of female rats to DAPM.

Thus, the preponderance of data collected here suggests that conjugation pathways, including acetylation, glucuronidation, and in particular, glutathione conjugation, are important detoxication pathways in DAPM metabolism. In addition, sex-dependent differences in the capacity of these pathways in the liver may explain the increased sensitivity of females to the hepatobiliary toxicity of DAPM. Ongoing studies in our laboratory are aimed at identifying the remaining DAPM metabolites observed by HPLC, as well as investigating the possible role of glycyl t-RNA synthetase in DAPM biotransformation in the liver.

ACKNOWLEDGMENTS

This work was supported by funds from the National Institute of Environmental Health Sciences (T32 ES07254, 1F32 ES05892, and ES06348), as well as the National Science Foundation (CHE-0518288, CHE-0630427) and the Louisiana Board of Regents (HEF(2001– 06)–08). We would like to thank Edward Ezell and David Polk and the Sealy Center for Structural Biology at the University of Texas Medical Branch for the use of their NMR instruments and their expert technical assistance.

BIBLIOGRAPHY

Bailey E, Brooks AG, Bird I, Farmer PB, Street B. Monitoring exposure to 4,4'-methylenedianiline by the gas chromatography-mass spectrometry determination of adducts to hemoglobin. Anal Biochem 1990;190:175–181. [PubMed: 2291463]

Bastian PG. Occupational hepatitis caused by methylenedianiline. Med J Aust 1984;141:533–535. [PubMed: 6482804]

Brooks LJ, Neale JM, Pieroni DR. Acute myocardiopathy following tripathway exposure to methylenedianiline. JAMA 1979;242:1527–1528. [PubMed: 470092]

Chen K, Dugas TR, Cole RB. Identification of metabolites of 4,4'-methylenedianiline in vascular smooth muscle cells by liquid chromatography-electrospray tandem mass spectrometry. J Mass Spectrom 2006;41:728–734. [PubMed: 16685702]

Clarke NJ, Rindgen D, Korfmacher WA, Cox KA. Systematic LC/MS metabolite identification in drug discovery. Anal Chem 2001;73:430A–439A.

Cocker J, Boobis AR, Davies DS. Determination of the N-acetyl metabolites of 4,4'-methylene dianiline and 4,4'-methylene-bis(2-chloroaniline) in urine. Biomed Environ Mass Spectrom 1988a;17:161–167. [PubMed: 3214672]

Cocker J, Brown LC, Wilson HK, Rollins K. A GC/MS method for the determination of 4,4'-diaminodiphenylmethane and substituted analogues in urine. J Anal Toxicol 1988b;12:9–14. [PubMed: 3352246]

Cocker J, Gristwood W, Wilson HK. Assessment of occupational exposure to 4,4'-diaminodiphenylmethane (methylene dianiline) by gas chromatography-mass spectrometry analysis of urine. Br J Ind Med 1986;43:620–625. [PubMed: 3756114]

Cocker J, Nutley BP, Wilson HK. A biological monitoring assessment of exposure to methylene dianiline in manufacturers and users. Occup Environ Med 1994;51:519–522. [PubMed: 7951775]

Dugas TR, Santa Cruz V, Liu H, Kanz MF. Evaluation of the gender differences in 4,4'-methylenedianiline toxicity, distribution, and effects on biliary parameters. J. Toxicol. Environ. Health. Part A 2001;62:467–483. [PubMed: 11289319]

Ellis MK, Hill S, Foster PMD. Reactions of nitrosonitrobenzene with biological thiols: Identification and reactivity of glutathion-S-yl conjugates. Chem.-Biol. Interactions 1992;82:151–163.

Eriani G, Delarue M, Poch O, Gangloff J, Moras D. Partition of tRNA synthetases into two classes based on mutually exclusive sets of sequence motifs. Nature 1990;347:203–206. [PubMed: 2203971]

Garg RP, Gonzalez JM, Parry RJ. Biochemical characterization of VlmL, a Seryl-tRNA synthetase encoded by the valanimycin biosynthetic gene cluster. J Biol Chem 2006;281:26785–26791. [PubMed: 16857674]

Hashimoto Y, Degawa M, Watanabe HK, Tada M. Amino acid conjugation of N-hydroxy-4-aminoazobenzene dyes: a possible activation process of carcinogenic 4-aminoazobenzene dyes to the ultimate mutagenic or carcinogenic metabolites. Gann 1981;72:937–943. [PubMed: 6804295]

Hobara T, Kobayashi H, Kawamoto T, Iwamoto S, Sakai T. Intestinal absorption of chloral hydrate, free trichloroethanol and trichloroacetic acid in dogs. Pharmacol. Toxicol 62:250–258. [PubMed: 3413026]88

Kanz MF, Dugas TR, Liu H, Santa Cruz V. Glutathione depletion exacerbates methylenedianiline toxicity to biliary epithelial cells and hepatocytes in rats. Toxicol Sci 2003;74:447–456. [PubMed: 12773769]

Kanz MF, Gunasena GH, Kaphalia L, Hammond DK, Syed YA. A minimally toxic dose of methylene dianiline injures biliary epithelial cells in rats. Toxicol Appl Pharmacol 1998;150:414–426. [PubMed: 9653073]

Kanz MF, Kaphalia L, Kaphalia BS, Romagnoli E, Ansari GA. Methylene dianiline: acute toxicity and effects on biliary function. Toxicol Appl Pharmacol 1992;117:88–97. [PubMed: 1440618]

Kanz MF, Wang A, Campbell GA. Infusion of bile from methylene dianiline-treated rats into the common bile duct injures biliary epithelial cells of recipient rats. Toxicol Lett 1995;78:165–171. [PubMed: 7618181]

Kato R, Yamazoe Y. Metabolic activation of N-hydroxylated metabolites of carcinogenic and mutagenic arylamines and arylamides by esterification. Drug Metab Rev 1994;26:413–429. [PubMed: 8082577]

Kautiainen A, Wachtmeister CA, Ehrenberg L. Characterization of hemoglobin adducts from a 4, 4'-methylenedianiline metabolite evidently produced by peroxidative oxidation in vivo. Chem Res Toxicol 1998;11:614–621. [PubMed: 9625729]

Klaassen CD, Watkins JB III. Mechanisms of bile formation, hepatic uptake, and biliary excretion. Pharmacol. Rev 36:1–67. [PubMed: 6144113]84

Kopelman H, Scheur PJ, Williams R. The liver lesion of the Epping jaundice. Quart. J. Med 35(140): 553–564.66

Lamb JC, Huff JE, Haseman JK, Murthy AS, Lilja H. Carcinogenesis studies of 4,4'-methylenedianiline dihydrochloride given in drinking water to F344/N rats and B6C3F1 mice. J Toxicol Environ Health 1986;18:325–337. [PubMed: 3712494]

Los LE, Welsh DA, Herold EG, Bagdon WJ, Zacchei AG. Gender differences in toxicokinetics, liver metabolism, and plasma esterase activity: Observations from a chronic (27-week) toxicity study of enalapril/Ditiazem combinations in rats. Drug Metab. Rev 24:28–33.96

Lynn RK, Garvie-Gould C, Milam DF, Scott KF, Eastman CL, Rodgers RM. Metabolism of the human carcinogen, benzidine, in the isolated perfused rat liver. Drug Metab Dispos 1983;11:109–114. [PubMed: 6133713]

Manson MM. Biphasic early changes in rat liver gamma-glutamyl transpeptidase in response to aflatoxin B1. Carcinogenesis 1983;4:467–472. [PubMed: 6132685]

McGill DB, Motto JD. An industrial outbreak of toxic hepatitis due to methylenedianiline. N Engl J Med 1974;291:278–282. [PubMed: 4407276]

Morgott DA. The *in vivo* biotransformation and acute hepatoxicity of methylenedianiline. Dissertation Abt. Int 45:531-B.84

Mugford CA, Kedderis GL. Sex-dependent metabolism of xenobiotics. Drug Metab. Rev 30:441–498. [PubMed: 9710703]98

Mulder GJ, Unruh LE, Evans FE, Ketterer B, Kadlubar FF. Formation and identification of glutathione conjugates from 2-nitrosofluorene and N-hydroxy-2-aminofluorene. Chem Biol Interact 1982;39:111–127. [PubMed: 7060218]

Mutlib AE, Chen H, Nemeth G, Gan L-S, Christ DD. Liquid chromatography/mass spectrometry and high-field nuclear magnetic resonance characterization of novel mixed diconjugates of the non-nucleoside human immunodeficiency virus-1 reverse transcriptase inhibitor, efavirenz. Drug Metab. Dispos 1999;27:1045–1056. [PubMed: 10460805]

Rao GS, Haueter G, Rao ML, Breuer H. Steroid glucuronyltransferases of rat liver. Properties of oestrone and testosterone glucuronyltransferases and the effect of ovariectomy, castration, and administration of steroids on the enzymes. Biochem. J 162:545–556. [PubMed: 869904]77

Skett P. Biochemical basis of sex differences in drug metabolism. Pharmac. Ther 38:269–304.88

Srivastava PK, Waxman DJ. Sex-dependent expression and growth hormone regulation of class alpha and class mu glutathione S-transferase MRNAs in adult liver. Biochem. J 294:159–165. [PubMed: 8363567]93

Sundseth SS, Waxman DJ. Sex-dependent expression and clofibrate inducibility of cytochrome P450 4A fatty acid ω–hydroxylases. J. Biol. Chem 267:3915–3921. [PubMed: 1740439]92

Weisburger EK, Murthy AS, Lilja HS, Lamb JC. Neoplastic response of F344 rats and B6C3F1 mice to the polymer and dyestuff intermediates 4,4'-methylenebis(N,N-dimethyl)-benzenamine, 4,4'-oxydianiline, and 4,4'-methylenedianiline. J Natl Cancer Inst 1984;72:1457–1463. [PubMed: 6587162]

Wu G, Fang YZ, Yang S, Lupton JR, Turner ND. Glutathione metabolism and its implications for health. J Nutr 2004;134:489–492. [PubMed: 14988435]

Zhu BT, Suchar LA, Huang MT, Conney AH. Similarities and differences in the glucuronidation of estradiol and estrone by UDP-glucuronyltransferase in liver microsomes from male and female rats. Biochem. Pharmacol 51:1195–1202. [PubMed: 8645343]96

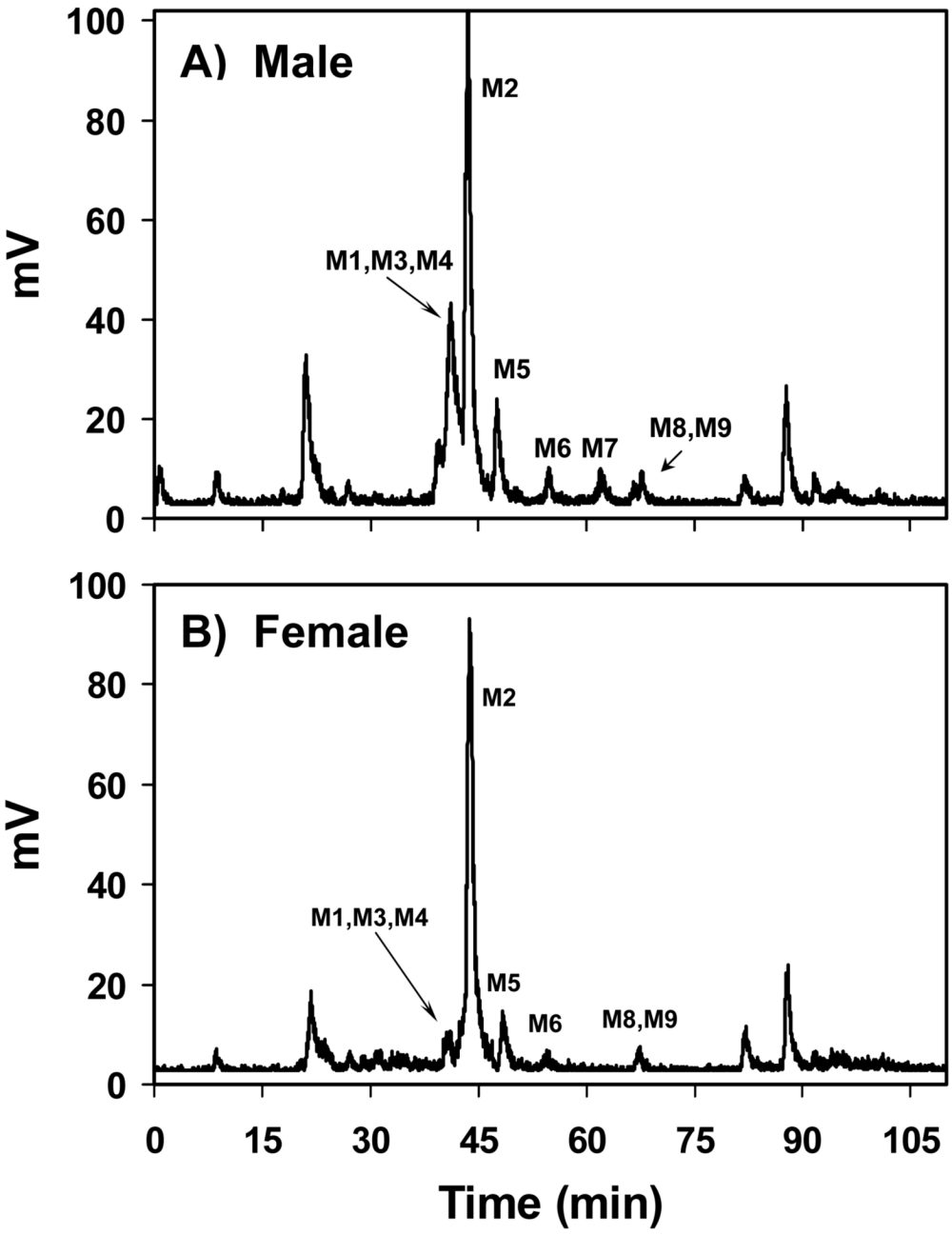

Figure 1.
Profile of radiolabeled metabolites detected using HPLC with radioisotope detection of bile samples from A) a male and B) a female rat, 1h after treatment with 25 mg/kg [^{14}C]-DAPM.

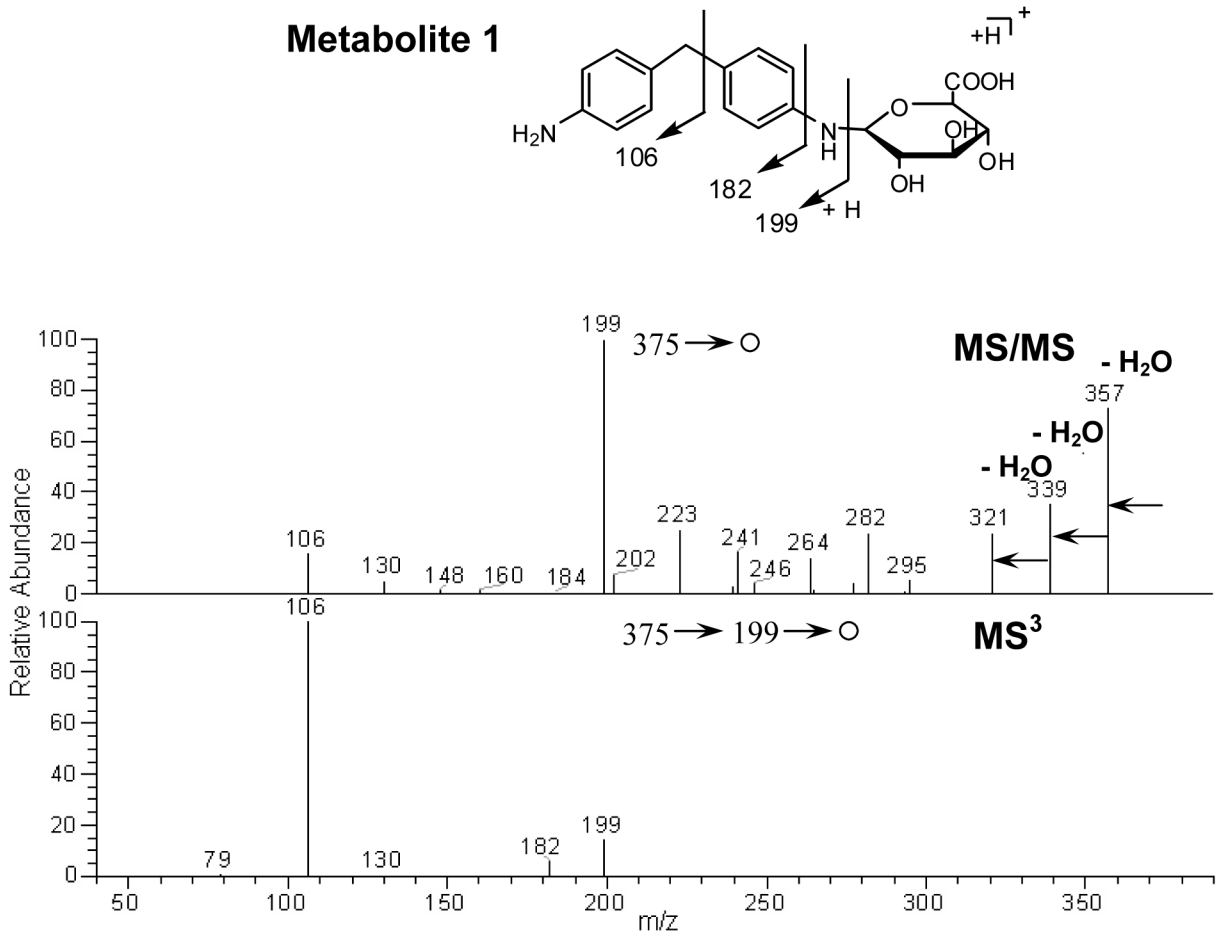

Figure 2.
MS/MS spectrum of protonated M1 precursor at m/z 375 Da and MS^3 spectrum of the fragment ion at m/z 199 Da.

A. MS/MS of Metabolite 2

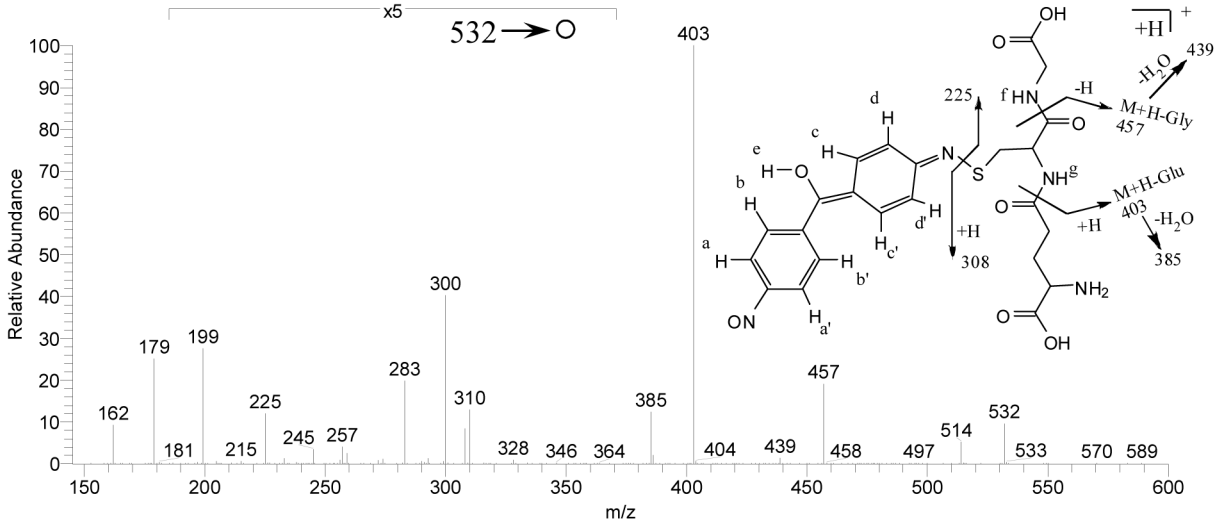

B. MS^3 of m/z 300 from Metabolite 2

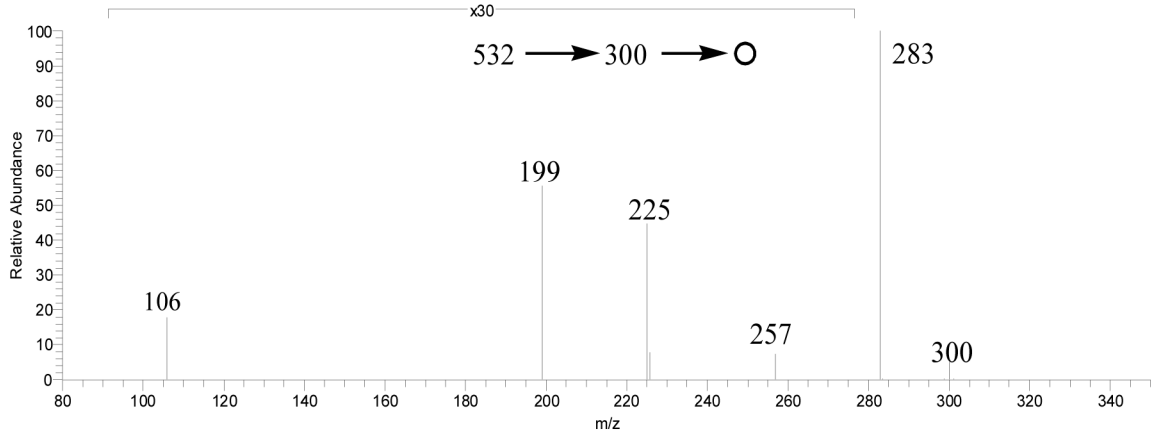

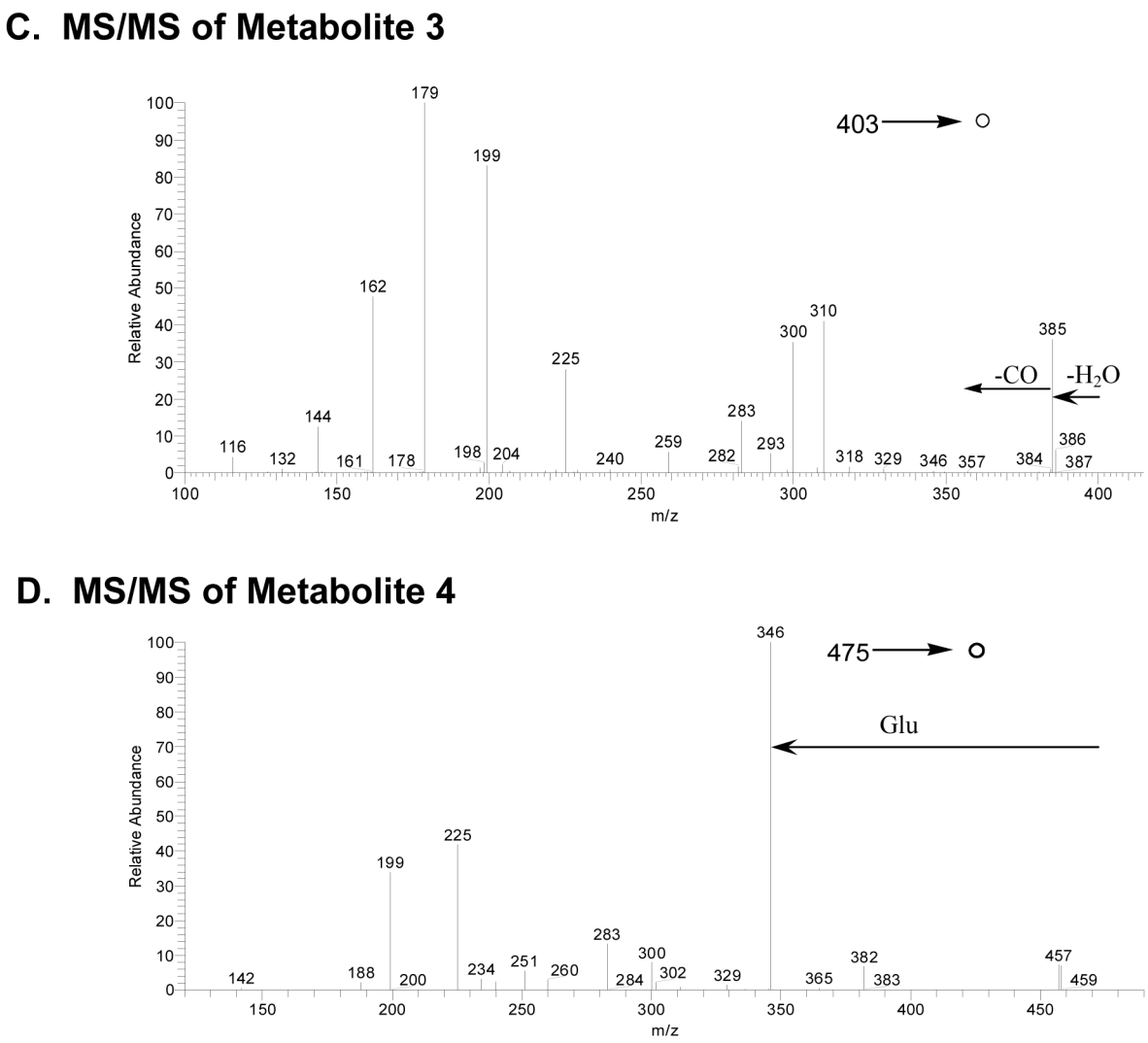

Figure 3.

A) MS/MS spectrum of the protonated glutathione conjugate M2 at m/z 532; B) MS^3 spectrum of the fragment ion at m/z 300; C) MS/MS of protonated cysteinyl-glycine conjugate M3 at m/z 403; and D) MS/MS of protonated glutamyl-cysteine conjugate M4 at m/z 475.

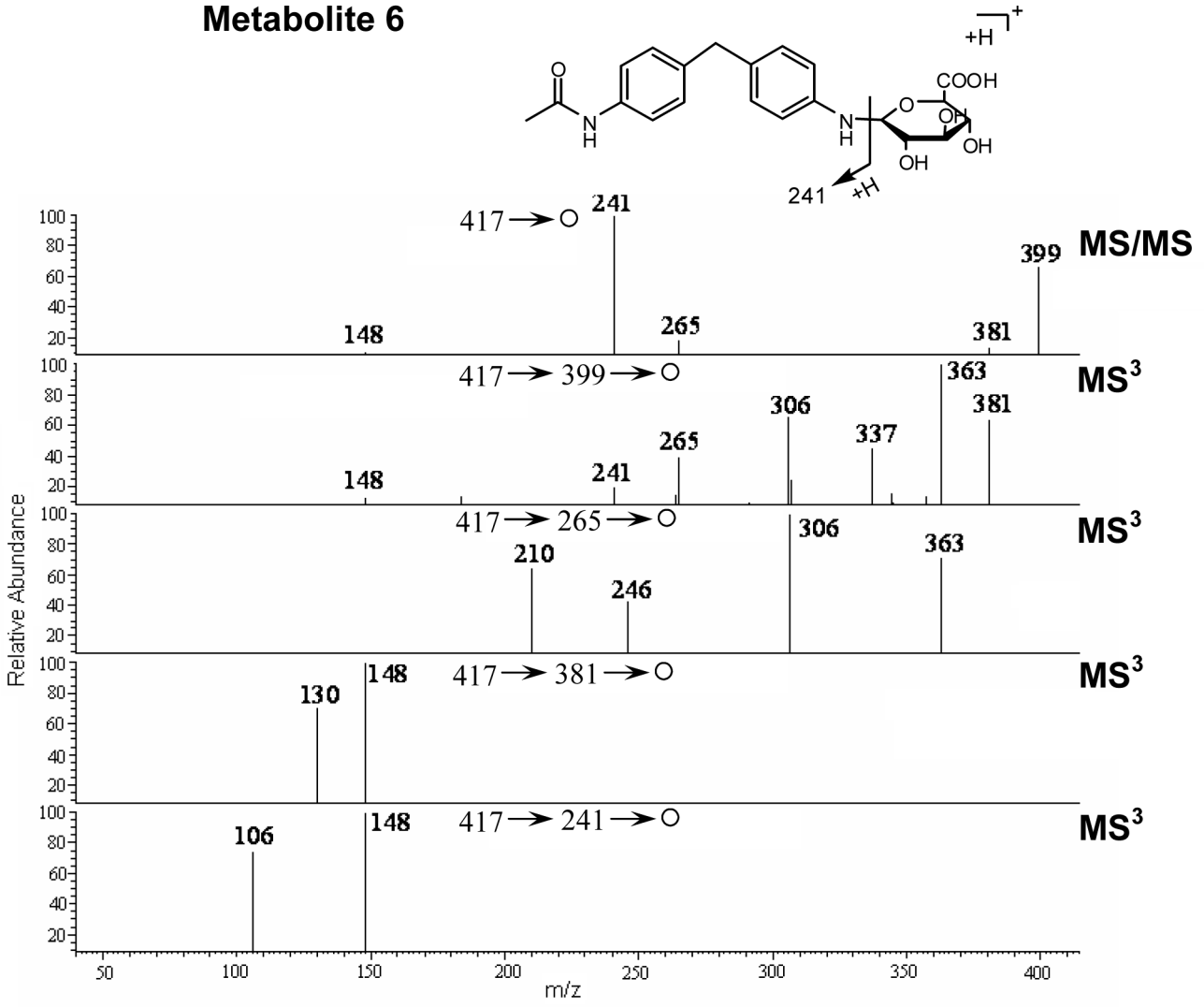

Figure 4.
MS/MS spectrum of protonated M6 at m/z 417 and MS^3 spectra of the fragment ions at m/z 399, 265, 381, and 241.

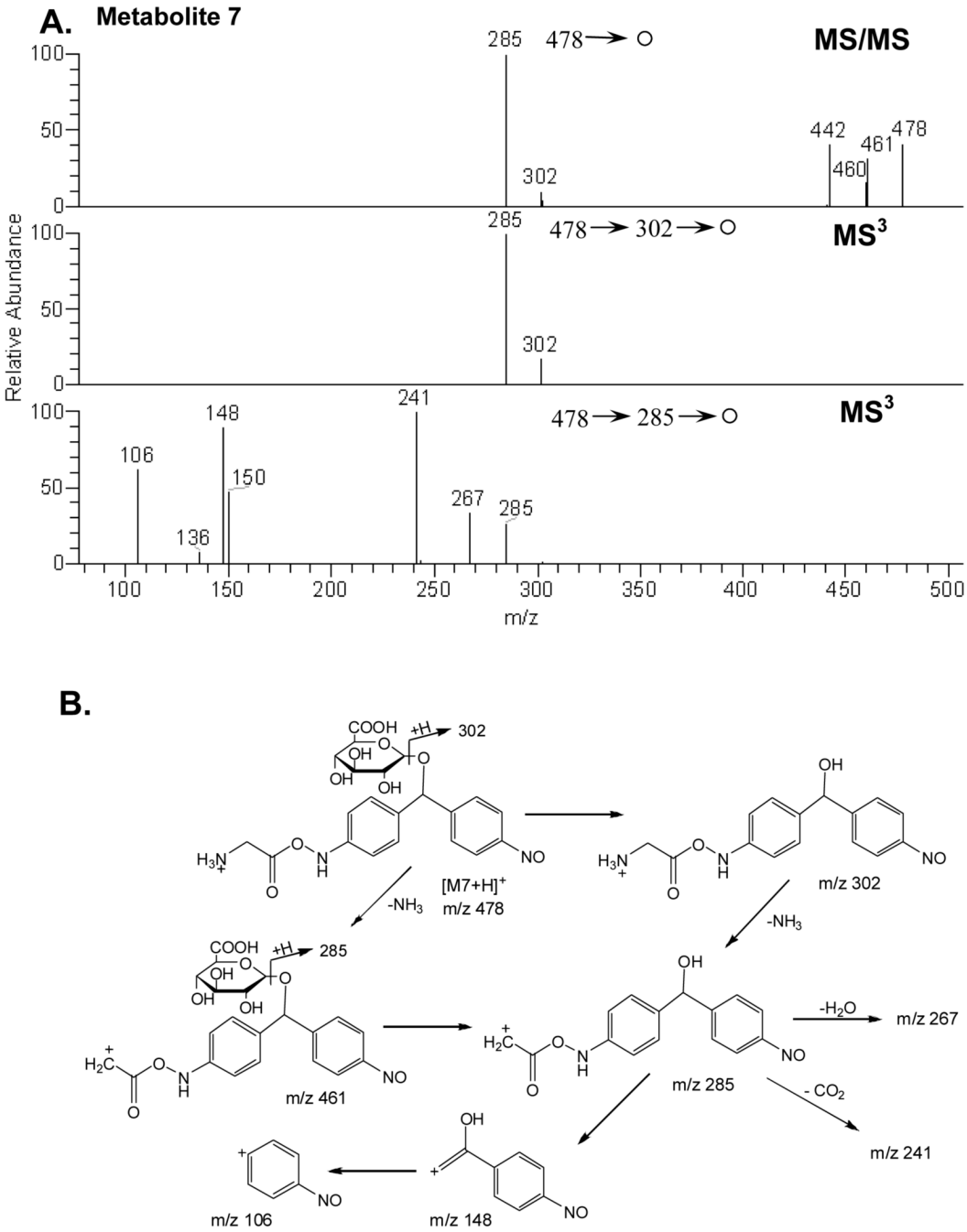

Figure 5.

A) MS/MS spectrum of protonated M7 at m/z 478 and MS^3 spectra of the fragment ions at 302, and 285; (B) Plausible fragmentation pathways of protonated M7.

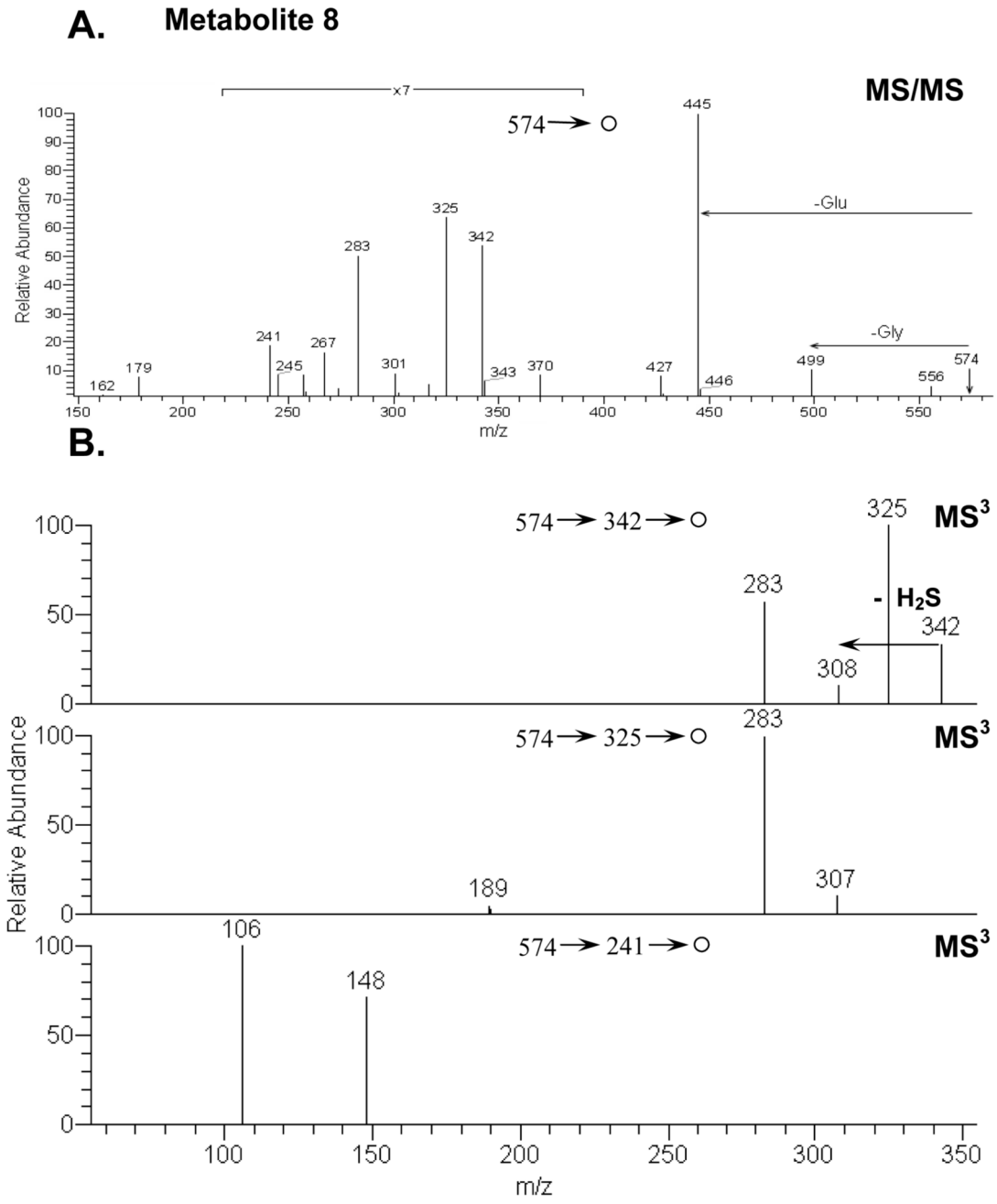

Figure 6.

A) MS/MS spectrum of the protonated glutathione conjugate M8 (m/z 574); (B) MS^3 spectra of the fragment ions of M8 at m/z 342, 325, and 241.

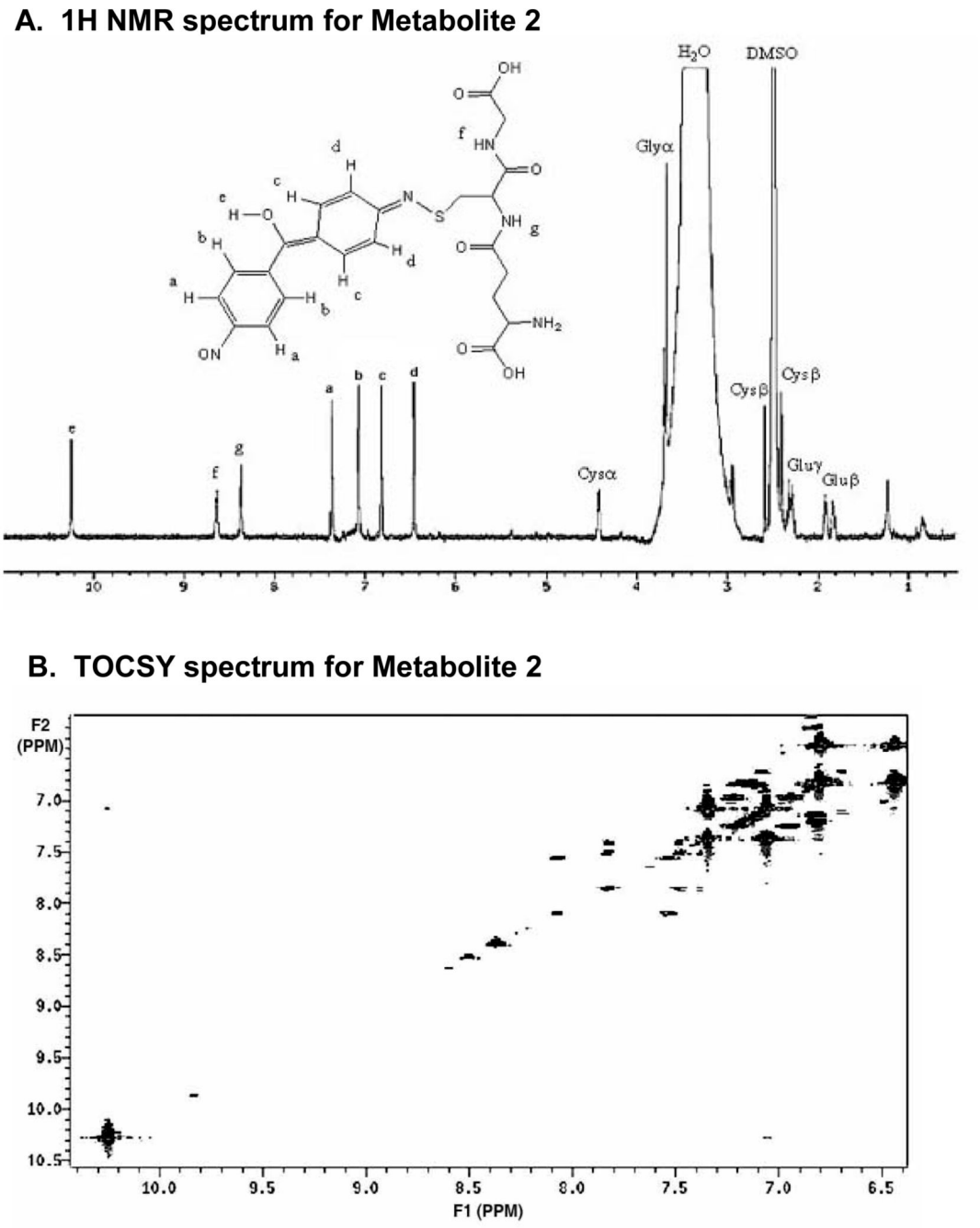

Figure 7.

A) ^{1}H NMR of the biliary glutathione conjugate (M2) eluting at 43.7 min on reversed-phase HPLC. B) Two-dimensional TOCSY NMR spectrum of M2, with arrows indicating the correlation between protons b (δ 7.0) and e (δ 10.2).

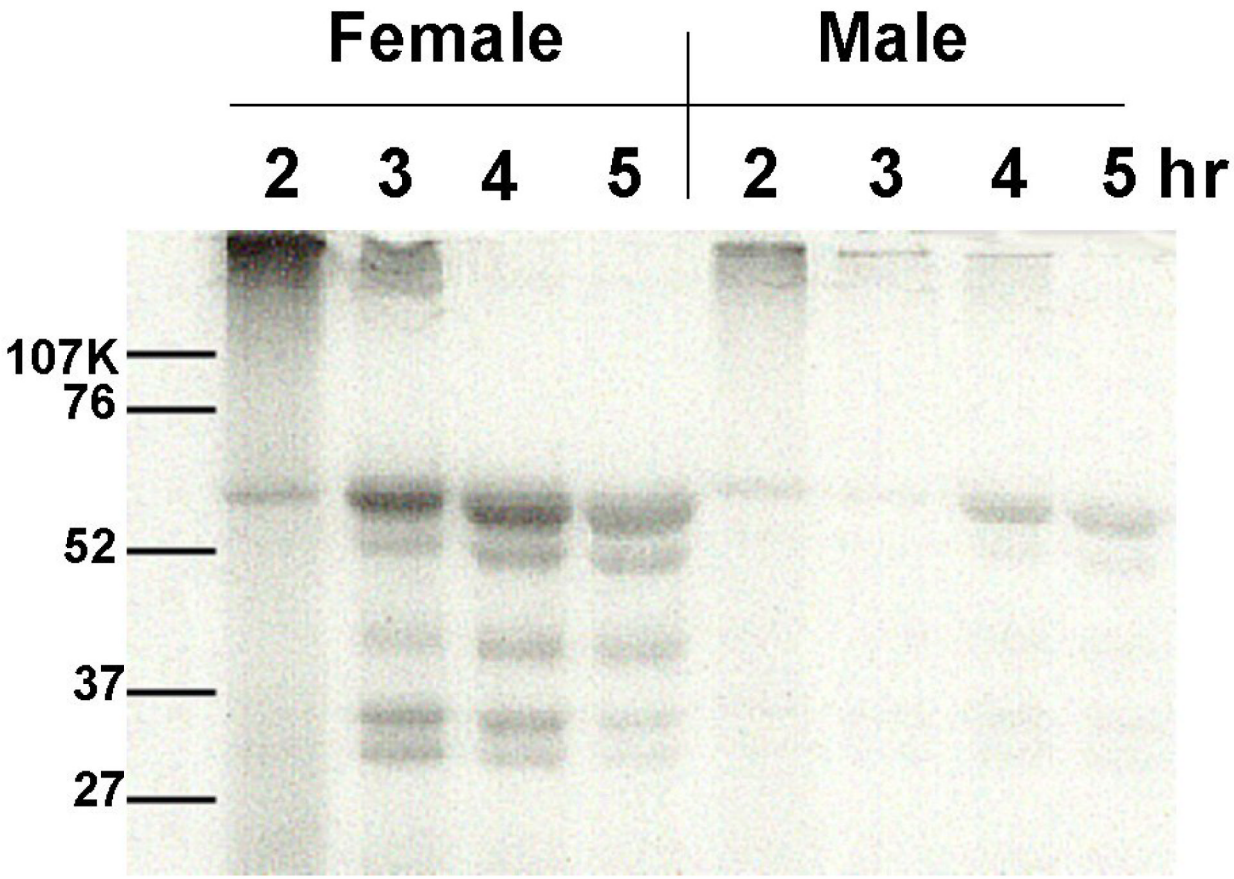

Figure 8.

Autoradiogram of SDS-PAGE showing radiolabeled protein in the bile of a male and a female rat 2 to 5h following a dose of 50 mg/kg [^{14}C]-DAPM. An equivalent amount of bile was loaded into each lane. Note that biliary protein concentrations were not different between the sexes within each time point, although protein concentrations increased with time for each animal.

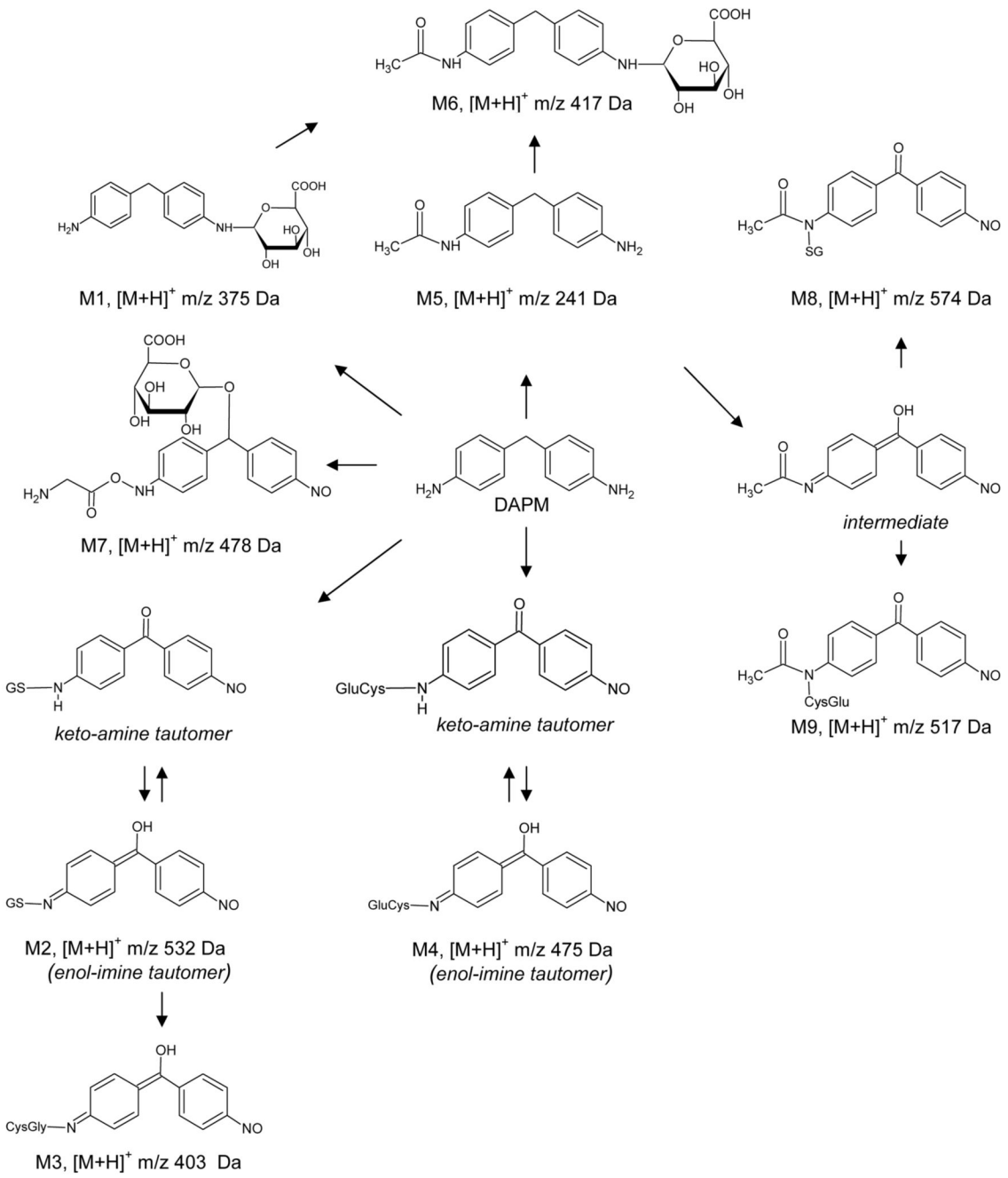

Scheme 1.

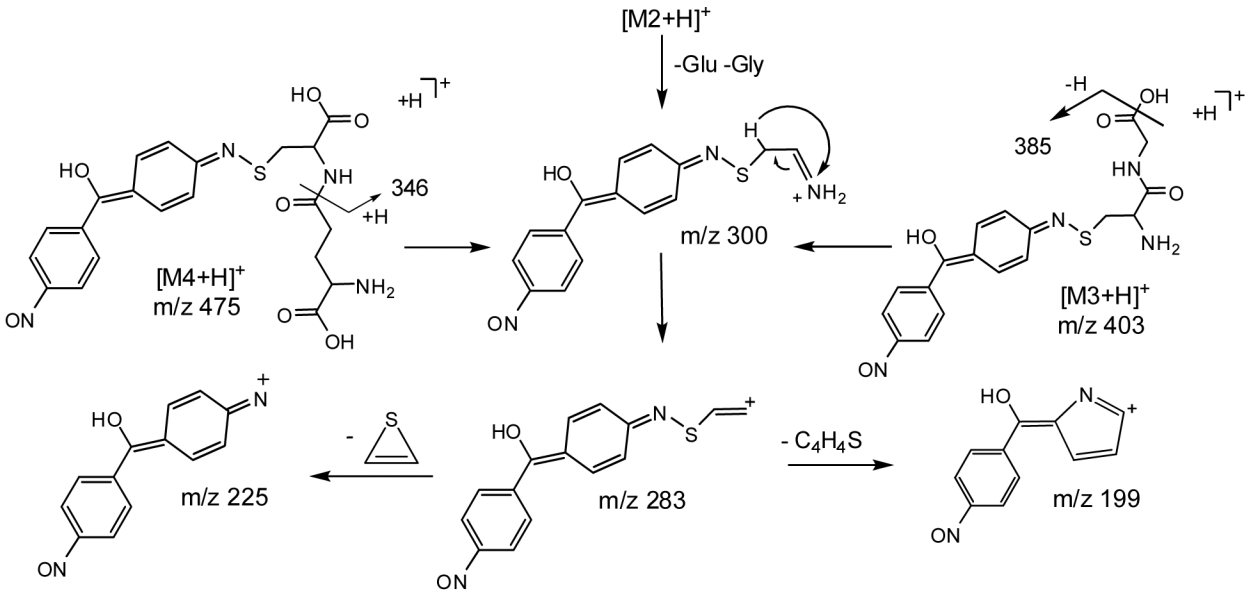

Scheme 2.

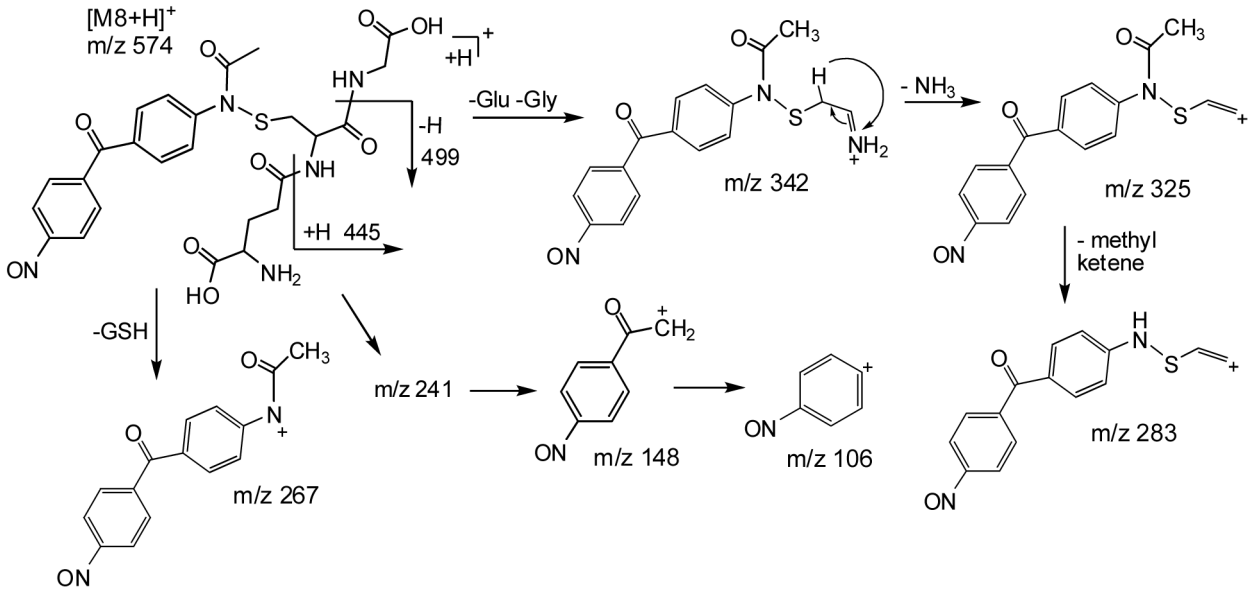

Scheme 3.

Table 1

Areas under the curve (AUC) for DAPM metabolite elimination in the bile.

Metabolite	HPLC t_r (min)	DAPM (mg/kg)	AUC (nmol*h)	
			Males	Females
DAPM	21.6**	25	155 ± 22	29 ± 14*
		50	176 ± 74	67 ± 31
M3/M4	40–41	25	367 ± 138	40 ± 29*
		50	127 ± 47	57 ± 33
M2	43.7	25	695 ± 193	224 ± 153
		50	654 ± 253	441 ± 250
M5	47.1	25	175 ± 11	39 ± 13*
		50	259 ± 86	132 ± 70
M6	54	25	112 ± 31	29 ± 22
		50	86 ± 19	26 ± 12*
M7	65–67	25	102 ± 31	13 ± 4*
		50	24 ± 6	45 ± 20

AUC were calculated for each rat and were averaged within treatment groups. Data represent means ± SEM for n=4–6 rats per group. Two-way ANOVA revealed significant differences between the sexes in all cases but M2. No significant effect of dose was detected within the sexes.

* Denotes significant differences between males and females at the same dose.

** Exhibited the same t_r as authentic DAPM, but MS characterization was unsuccessful, due to poor ionization.